



*Proceedings of the
Annual Stability Conference
Structural Stability Research Council
Baltimore, Maryland, April 10-13, 2018*

Stability Analyses for a Multi-Span Tied Steel Arch Bridge: AASHTO Effective Length Method, Eigenvalue Analysis and AISC Direct Analysis Method

Jonathan Eberle¹, Soham Mukherjee², Paul Kettleson³, Daniel Baxter⁴, and Alexandra Willoughby⁵

Abstract

The Smith Avenue Bridge (High Bridge), spanning the Mississippi River in St. Paul, Minnesota, consists of 3 continuous tied steel arch spans measuring 282'-3", 520' and 241'-9". Originally constructed in 1987, the bridge is currently undergoing comprehensive rehabilitation including the replacement of its original concrete deck. In support of the rehabilitation design, the Minnesota Department of Transportation (MnDOT) tasked AECOM with load rating of the arch spans. Early in the design, AECOM recognized the conservatism inherent in the simplified Effective Length Method utilized for arch rib axial capacity calculations within the AASHTO LRFD Bridge Design Specifications. As permitted by AASHTO LRFD, AECOM employed eigenvalue analysis as a more refined means to determine the critical buckling load for the arch rib. Additionally, MnDOT selected a peer review team (Michael Baker International) to perform an independent analysis for verification of the eigenvalue approach. The peer reviewer utilized the Direct Analysis Method found in Chapter C of the AISC Steel Construction Manual, another refined analysis method, to load rate the arch rib. The increase in axial capacity gained by the eigenvalue analysis conducted by AECOM allowed the arch rib to rate for current AASHTO design loadings as well as MnDOT permit vehicles and was shown to be conservative by the results of the Direct Analysis Method conducted by Michael Baker. A comparison of the results determined using the AASHTO Effective Length Method, AASHTO method employing eigenvalue analyses and the Direct Analysis Method is presented in this paper.

¹ Structural Engineer, AECOM, <jonathan.eberle@aecom.com>

² Structural Engineer, AECOM, <soham.mukherjee@aecom.com>

³ Project Manager, MnDOT, <paul.kettleson@state.mn.us>

⁴ Senior Bridge Engineer, Michael Baker International, <dbaxter@mbakerintl.com>

⁵ Bridge Engineer, Michael Baker International, <Alexandra.willoughby@mbakerintl.com>

1. Introduction

1.1 Background

The High Bridge consists of a 3-span open spandrel steel tied deck arch main spans with steel multi-girder approach spans. The bridge consists of eleven spans totaling 2755 ft. in length. The bridge was opened in 1987, replacing a previous bridge at the same location. The main river spans are supported by a 3-span tied arch, consisting of a full arch (Span 4) spanning 520 ft. with 2 half arches on each side of Span 4, measuring 282 ft. 3 in. and 241 ft. 9 in. for Spans 3 and 5, respectively. The plan and elevation of the High Bridge are shown in Fig. 1.

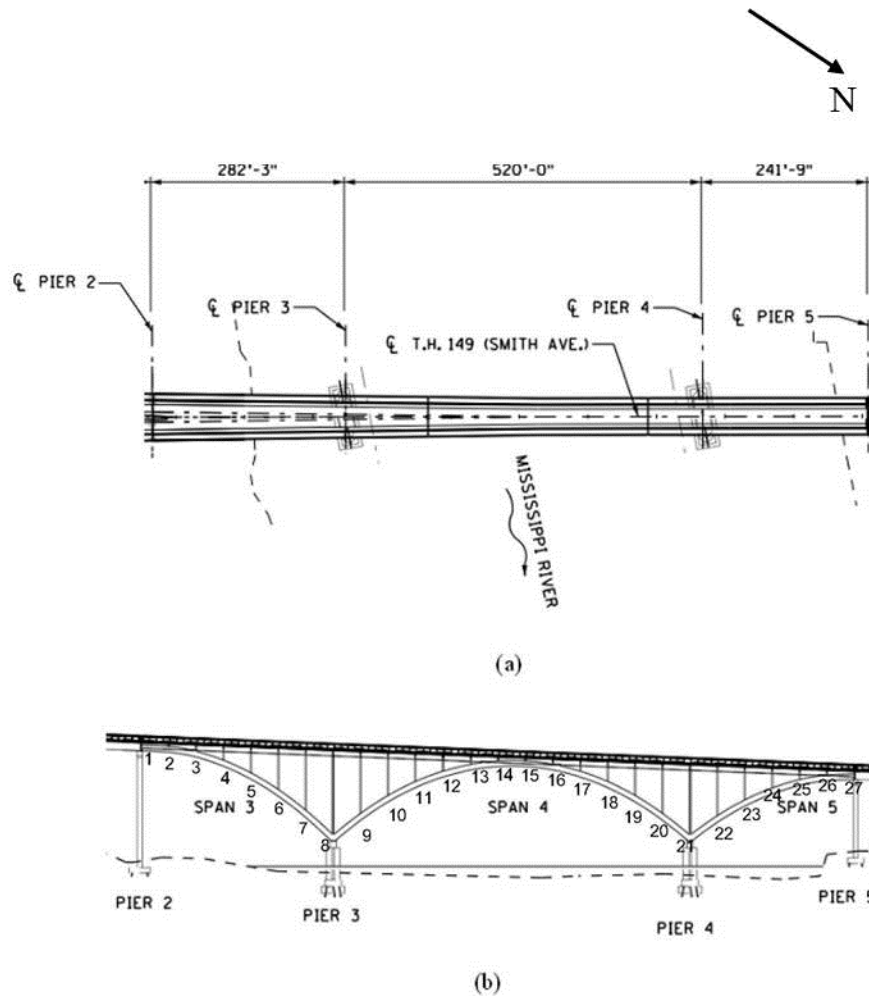


Figure 1: High Bridge: (a) Plan; (b) Elevation (Panel Numbering Shown)

The arch spans consist of two arch ribs spaced transversely at 36' - 0". The arches will be referred as east arch and west arch in subsequent texts and figures. The arch ribs are built up steel box sections, with two varied cross sections, a larger box section for the main portion of Spans 3 and 5, and a smaller box section for the remainder of Spans 3 and 5 and all of Span 4. The webs of the box sections are 8 ft deep by 1 in. thick plates and the flanges are 3 ft wide by 2 in. thick for the larger box section and 3 ft wide by 1 1/8 in. thick for the smaller box section. The arch ribs are stiffened with four WT sections welded to the inside of the webs. The arch rib sections are shown in Fig. 2.

The top flanges of the arch ribs are connected through gusset plates to spandrel columns located at panel points spaced at 40' – 0". The spandrel columns then support the floor system of the concrete deck unit consisting of stringers and floorbeams. The arch span deck width is variable – ranging from 54' – 4" to 68' – 10", out-to-out. Two relief joints exist in the deck within the arch spans, both located in Span 4 with one joint adjacent to Panel Point 11 and the other adjacent to Panel Point 19. The number of the stringers in the cross-section changes at the location of the south deck relief joint, with six stringers north of the joint and seven stringers south of the joint.

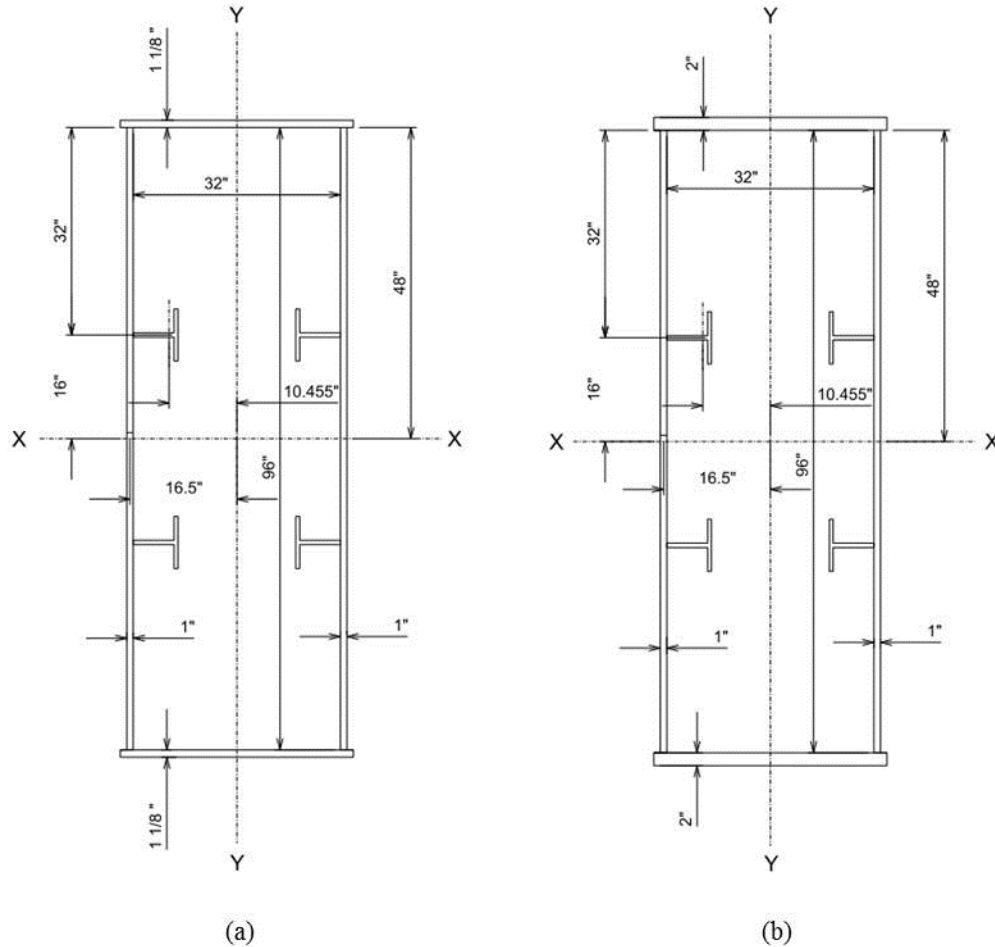


Figure 2: Arch Rob Box Sections: (a) Section with 1 1/8 in. Flange; (b) Section with 2 in. Flange

Due to deteriorating bridge deck condition, comprehensive rehabilitation of High Bridge including complete replacement of its original concrete deck was deemed necessary by MnDOT, the owner of the bridge. As a part of the rehabilitation project, MnDOT tasked AECOM with load rating of the arch spans, to identify any strengthening requirements to satisfy current design specifications and ensure that the structure rates for current design and permit live loads.

1.2 Project Scope

The ratings were performed in accordance with the AASHTO LRFR methodology, as outlined in the AASHTO LRFD Bridge Design Specifications (AASHTO LRFD 2014), the AASHTO Manual for Bridge Evaluation (AASHTO MBE 2011), and the MnDOT LRFD Bridge Design Manual (MnDOT 2015). The rating factors were determined by the Engineer of Record (EOR) for inventory and operating ratings for three cases 1) the originally constructed condition of the bridge with no condition or system factors included 2) the existing condition of the bridge with applicable condition and system factors and 3) the proposed condition of the bridge with new deck, strengthening and with appropriate condition and system factors. Discussed herein for comparison purposes are the ratings factors for the proposed condition of the bridge with new deck, strengthening and with appropriate condition and system factors which were confirmed by the Peer Review team. Additionally, the arch span superstructure was analyzed for the sequential stages of the deck removal and reconstruction, and the member demands were checked against the latest provisions of the specifications. The results of the deck removal and reconstruction sequence are beyond the scope of this paper.

The long main spans of the High Bridge are dominated by the dead load. As the dead loads are approximately uniform, these loads create significant axial compression in the arch ribs. Thus, the arch ribs under high axial compression become a critical member for load rating of the arch spans. Initially, the axial load capacities of the steel box arch rib sections were determined using the simplified Effective Length Method as outlined in the AASHTO LRFD 2014 (similar to the method used for the original design). This approach employs the Euler buckling equation to determine the critical buckling load or Euler buckling load. However, the conservatism built in the method resulted in relatively low axial capacities and a subsequent unsatisfactory rating factor by the AASHTO MBE code. To more accurately determine the axial capacity, eigenvalue analysis was used to determine the critical buckling load for the arch rib. To verify the eigenvalue analysis method used, a peer review team (Michael Baker International) was selected by MnDOT. The peer reviewer utilized the Direct Analysis Method found in the AISC 360-16 *Specification for Structural Steel Buildings* (AISC 2016) to load rate the arch rib. The increase in axial capacity gained by the eigenvalue analysis allowed the arch rib to rate for current AASHTO design loadings as well as MnDOT permit vehicles, and was shown to be conservative by the results of the Direct Analysis Method conducted by the peer reviewer. The study provided valuable insight to the conservatism in the simplified capacity calculation methods provided in AASHTO LRFD and established a novel way to analyze multi-span arch bridges for determination of the critical buckling load.

2. AASHTO Effective Length Method

2.1 Determination of Buckling Load

Global buckling of a member happens when the member in compression becomes unstable due to its slenderness (ratio of member unbraced length to radius of gyration = KL/r) as subjected to an applied load. The Euler buckling formula for critical buckling load or Euler buckling load is derived for an ideal case where the member is long, slender, homogenous, elastic, and is subjected to concentric axial load. The AASHTO Effective Length Method (AASHTO LRFD 2014) utilizes the Euler buckling formula (Eq. 1) to determine the critical buckling load, P_c , where K is the effective length factor and l_u is the unsupported length of a compression member. AASHTO defines the unsupported length of the compression member as one half of the length of the arch rib (measured along the arch rib).

$$P_e = \frac{\rho^2 EI}{(Kl_u)^2} \quad (1)$$

This method requires a K value to be selected from Table 4.5.3.2.2c-1 which defines K values given the arch rise to span ratio and an assumption of the arch fixity (2 hinge, 3 hinge or fixed). For a simple span arch with fixities that match one of the cases given in the table, this method would be expected to provide an accurate critical buckling load based upon the research used to develop this table. However, for the High Bridge, the continuous nature of the structure prevents it from fitting into any of the fixity conditions provided. To use this method, an assumption needs to be made regarding the fixity of the spans. To avoid an unconservative approach, the main span was approximated as a two hinge arch, neglecting the restraint provided at piers 3 and 4 by the side spans. The side spans were approximated as a 3 hinge arch, again neglecting any restraint provided by the main span. Although this approach would be considered conservative, it was recognized that the long slender piers at the outside of the arch span unit coupled with the flexibility of the post tensioned ties allow for displacement of “crown” of the side spans thus leading to an anticipated decrease in critical buckling load. As described earlier, Span 4 is a full arch with a span of 520 ft and a rise of 109.35 ft leading to a rise to span ratio of 0.21. Spans 3 and 5 are half arches with span lengths of 282 ft. 3 in. and 241 ft. 9 in. respectively, and rises of 131.75 ft. and 90.15 ft. respectively. This leads to rise to span ratios of 0.23 and 0.19 for Spans 3 and 5, respectively. The K values determined from Table 4.5.3.2.2c-1 of AASHTO LRFD Bridge Design Specifications are shown in Table 1.

2.2 Axial Capacity of Arch Ribs by AASHTO Effective Length Method

To calculate the compression capacity of the arch rib using AASHTO, Eqns. 6.9.4.1.1-1 and 6.9.4.1.1-2 were used. These equations calculate the nominal capacity as a function of the elastic critical buckling resistance (calculated using the Euler buckling equation previously discussed) and the equivalent nominal yield resistance. The equivalent nominal yield resistance is defined in AASHTO as the yield resistance of the section times a slender element reduction factor to account for local buckling effects. In lieu of the simplified methods outlined in AASHTO, the arch ribs were checked for local buckling by modelling a section of the arch rib using a finite element mesh (Fig. 3) between diaphragms using LUSAS. The arch rib section with the smaller flange sizes and larger unbraced length was modelled to create the worst buckling scenario. One end of the arch rib was given a fixed for translation boundary condition, and a total load of 100 kip was applied uniformly at the other end over the entire cross section of the arch rib. The applied load resulted in a uniform stress of 0.33 ksi. The eigenvalue analysis was performed, and the first eigenvalue calculated was 246.1 with the mode shape shown in Fig. 3. To determine the critical buckling load for local buckling, the eigenvalue was multiplied by the uniform applied stress which results in a critical buckling stress of 81.7 ksi which was significantly higher than the yield stress of 50 ksi. The analysis shows that the arch rib will yield before any local buckling occurs and thus no reduction factor for local buckling is required. Accordingly, the slender element reduction factor was taken as 1.0 while calculating the axial capacity. The buckling mode shape is shown in Fig. 3.



Figure 3: Deflected Arch Rib Model for Local Buckling Analysis

The Euler buckling loads for the arch ribs in each span were calculated using Eq. 1, and were used to calculate the nominal compressive resistance of the arch rib sections using Equations 6.9.4.1.1-1 and 6.9.4.1.1-2 of AASHTO (AASHTO LRFD 2014). The K values, the Euler buckling loads (P_e) and the factored axial capacities (P_r) of the arch ribs sections are tabulated in Table 1. The buckling loads determined using the Euler buckling formula resulted in relatively low axial capacities, which resulted in unsatisfactory rating factors.

Table 1: Euler Buckling Loads and Factored Axial Capacities by AASHTO Effective Length Method

Span	Section	K	P_e (kips)	P_r (kips)
Span 3	1 1/8" Flange	1.13	5313	4659
Span 3	2" Flange	1.13	7703	6755
Span 4	1 1/8" Flange	1.10	6822	5978
Span 5	1 1/8" Flange	1.16	7451	6463
Span 5	2" Flange	1.16	10804	8994

3. Refined Eigenvalue Analysis

3.1 Determination of Buckling Load

A need for refined methods of capacity calculation was defined early in the project. To allow for the capacity equations found in AASHTO to be used, the option to employ advanced methods of analysis for determining the critical buckling load, as outlined in AASHTO LRFD C6.9.4.1.1, was exercised. Eigenvalue analysis was used to accurately determine the critical buckling load of the arch rib for the structural system of interest. These more accurate critical buckling loads subsequently result in less conservative and more accurate buckling loads than determined by the AASHTO (AASHTO 2014) Effective Length Method. However, existing literature (Ziemian 2010, Nittleton 1977, and Bridge Engineering Handbook 2000) was focused on single span arches where the critical buckling load was determined by loading the arch with uniform load applied full length which creates a case of approximate pure axial bending in the arch rib. This concept was not readily applicable to High Bridge because for a span of a continuous arch, the load on adjacent spans has a stabilizing effect on the span of interest. As no guidance was available for loading of continuous arches, a conservative approach was taken wherein the self-weight of the arch spans was applied to the structure which is approximately a uniform load and then a uniformly distributed load was applied to each span individually and incrementally increased until buckling occurred within the arch rib.

The eigenvalue analysis approach is based on analyzing the structure under a given applied load and the analysis program determines a set of load multipliers that correspond to different buckling loads. The lowest multiplier corresponds to the first mode of buckling. The value of this multiplier, or the first eigenvalue, indicates that if all loads on the structure are multiplied by the eigenvalue, the structure will become unstable. The critical buckling load is then determined as the result of multiplying the compressive axial load in the critical rib member under the applied loads by the first eigenvalue. Based upon available guidance, the axial load in the critical member is taken as the axial force at the quarter point of the arch span. For the High Bridge, the critical load was taken as the lower of the axial forces at the quarter points of the main span or the axial force at the midpoint of the side spans (because they are half arch spans).

Eigenvalue analyses were conducted for the three models as indicated. Because the eigenvalue analysis produces a multiplier that should be applied to all loads and it was the intent not to amplify dead loads or the loads within the post-tensioned tie, an iterative approach was necessary. The uniform load applied to the span of interest (applied as a horizontal projection of distributed load as shown in Fig. 4 for Span 4) was incremented until the eigenvalue for the first mode was equal to 1.0. This means that the structure becomes unstable under the dead load applied to the full length of the bridge plus the additional load applied to the span of interest. For each of the three analyses, the buckling was initiated in the loaded span (see Fig. 4) and the critical buckling load was assumed equal to the axial load at the following point (see Fig. 5):

- Span 4 loaded: The axial load at the controlling quarter point (quarter point with lower axial force) of Span 4 was taken to be the critical buckling load.
- Spans 3 and 5 Loaded: The axial load at the midpoint of the loaded span of interest was taken to be the critical buckling load for the given span.

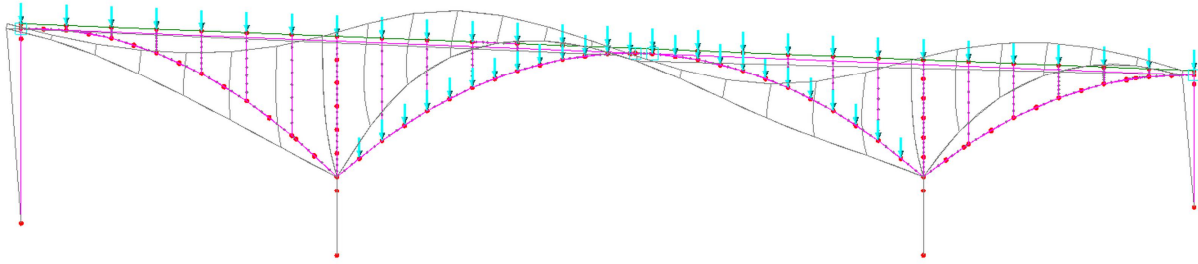


Figure 4: Buckling Mode Shape for Span 4

Location where Critical Buckling Load is Measured

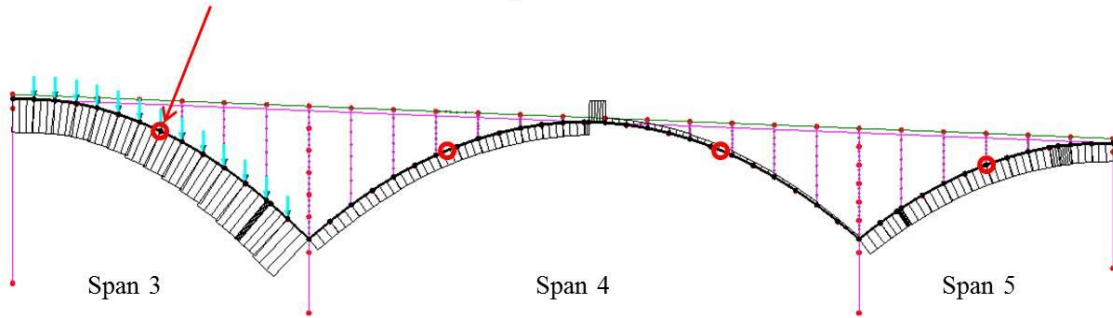


Figure 5: Location of Axial Load Measurements

3.2 Axial Capacity of Arch Ribs by Eigenvalue Analysis

The critical buckling loads for the arch ribs in each span were determined through the eigenvalue analysis, and were used to calculate the nominal compressive resistance of the arch rib sections using Equations 6.9.4.1.1-1 and 6.9.4.1.1-2 of AASHTO (AASHTO LRFD 2014). As described earlier in Section 2.2, the slender element reduction factor was taken as 1.0 because local buckling was shown to not occur within the arch rib. The critical buckling loads (P_e) and the factored axial capacities (P_r) of the arch ribs sections are tabulated in Table 2. The buckling loads determined using the refined analysis resulted in significantly higher axial capacities and allowed the arch rib to rate for current AASHTO (AASHTO 2014) design loadings as well as MnDOT (MnDOT 2015) permit vehicles.

Table 2: Critical Buckling Loads Factored Axial Capacities by Eigenvalue Analysis

Span	Section	P_e (kips)	P_r , Eigenvalue (kips)	P_r , Effective Length Method (kips)
Span 3	1 1/8" Flange	8898	7046	4659
Span 3	2" Flange	8898	7346	6755
Span 4	1 1/8" Flange	17297	9940	5978
Span 5	1 1/8" Flange	8714	6941	6463
Span 5	2" Flange	8714	7214	8994

4. Direct Analysis Method

4.1 Selection of Analysis Method and Software

To verify the work of the Engineer of Record (EOR), the Michael Baker International peer review team elected to conduct a load rating of the arch spans using an alternative method that did not include eigenvalue buckling analysis. Eigenvalue analysis will typically provide upper-bound solutions to stability problems, while the buckling loads provided by geometric-nonlinear analysis will usually be lower. The peer review team consequently elected to load rate the High Bridge arch spans using geometric-nonlinear analysis to evaluate stability of the arch and compute second-order effects.

Analysis of structures for buckling using geometric-nonlinear analysis is not currently codified in the AASHTO *LRFD Bridge Design Specifications*. However, the current July 7th, 2016 edition of the ANSI/AISC 360-16 *Specification for Structural Steel Buildings* (AISC 2016) does provide provisions for conducting geometric-nonlinear buckling analysis. These provisions are listed in code sections Section C1 and Appendix 1: Design by Advanced Analysis, and comprise the AISC Direct Analysis Method of Design. The peer review team followed the AISC code provisions for geometric-nonlinear analysis with elastic material properties. Key portions of these specifications include:

- “The analysis shall consider geometric nonlinearities, including P-D, P-d and twisting effects as applicable to the structure” (pp. 16.1-186).
- “In all cases, the analysis shall directly model the effects of initial imperfections due to both...system imperfections, and...member imperfections” (pp. 16.1-186).
- Suggested nodal geometry imperfections are a 1/500 maximum out-of-plumbness ratio, and a 1/1000 maximum out-of-straightness of members ratio (pp. 16.1-186).
- “A factor of 0.80 shall be applied to all stiffnesses that are considered to contribute to the stability of the structure. It is permissible to apply this reduction factor to all stiffnesses in the structure” (pp. 16.1-26).
- When the Design by Advanced Analysis provisions are followed, “the nominal compressive strength of members, P_n , may be taken as the cross-section compressive strength $F_y A_g$, or as $F_y A_e$ for members with slender elements” (pp. 16.1-187).

There are therefore two significant differences between following the AISC Advanced Analysis approach and a conventional linear-elastic analysis approach to determine High Bridge arch rib demands and capacities. The first difference is that for a linear-elastic approach, second-order effects would be approximated using AASHTO LRFD moment magnification provisions, while for AISC Advanced Analysis, second-order effects are computed directly by the analysis software. The second difference is that in a linear-elastic analysis, axial capacity would be determined by using capacity equations that include the elastic critical buckling resistance P_e , while for AISC Advanced Analysis, axial resistance is taken as the compressive yield strength of the member for members without slender elements. (The High Bridge arch rib sections are not slender). Taking axial capacity as the yield strength instead of the buckling strength is possible because the analysis software monitors the structure for loss of stability caused by buckling.

One difference between the AISC Advanced Analysis approach and the eigenvalue analysis performed by the EOR is that the elastic critical buckling resistance P_e determined from eigenvalue analysis by the EOR was used in the AASHTO LRFD code equations for axial

capacity, while the peer review team followed the AISC Advanced Analysis provisions to determine axial capacity, ($F_y A_g$) for the arch load rating.

To meet the requirements of AISC Appendix 1: Design by Advanced Analysis, software must be capable of both correctly computing second-order effects, and monitoring the structure for loss of stability caused by buckling. The peer reviewer selected MIDAS/Civil as the analysis program for geometric-nonlinear analysis of the High Bridge. To validate that MIDAS/Civil meets the requirements of AISC Appendix 1, two benchmark verification problems given in AISC 2016 were performed. Based on these results, the peer reviewer determined that MIDAS/Civil can accurately compute geometric-nonlinear behavior and critical loads and displacements as required by AISC Appendix 1. A screenshot of the 3D MIDAS/Civil analysis model of the High Bridge arch spans is shown in Figure 6.

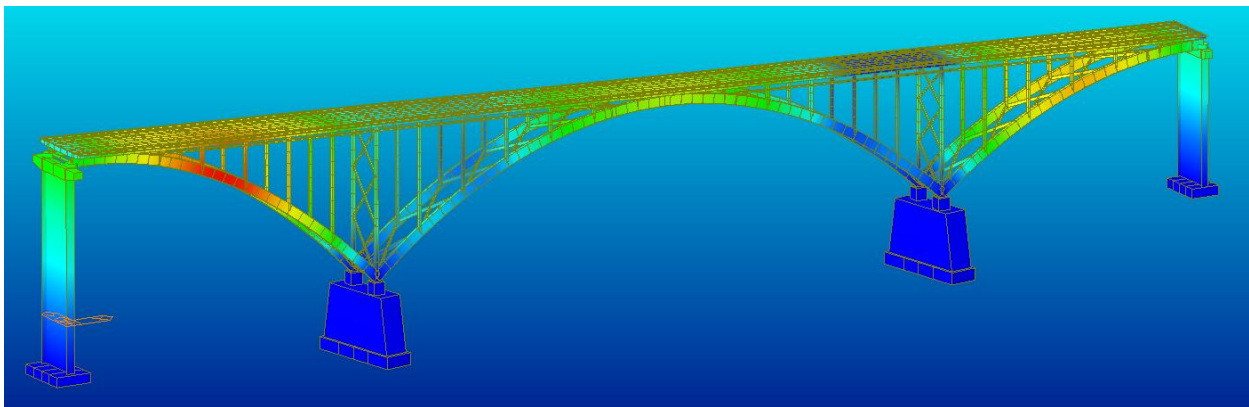


Figure 6: MIDAS/Civil 3D model of the High Bridge arch spans

4.2 Load Rating the Arch Using AISC Appendix 1: Design by Advanced Analysis

The AISC Appendix 1 provisions were only used by the peer reviewer to determine ratings for arch rib panels that had demand-capacity ratios above 1.0 from a conventional linear-elastic analysis using the AASHTO LRFD axial capacity equations. The screening for locations failing a linear-elastic analysis was accomplished by considering concurrent force results for three live load scenarios for the HL-93 and owner-specified permit rating vehicles: maximum strong axis moment, minimum strong axis moment, and maximum compressive axial force. Then, the concurrent force live load scenario that resulted in the maximum demand-capacity ratio at each panel not passing the screening was chosen for further analysis using AISC Appendix 1 procedures. The moving load tracer (MLT) function within MIDAS/Civil was used to generate equivalent static live load cases that produced the controlling force effects at each panel.

For each panel that did not pass the linear-elastic screening, the governing static live load case was then imported into a 3D MIDAS/Civil model of the structure that had been configured with the initial imperfection and reduced modulus of elasticity provisions specified by AISC Appendix 1 for geometric-nonlinear analysis. A total factored static load case for each panel was then created within MIDAS/Civil that included all dead loads, tendon loads, and the governing live load. This was required since superposition of force results is not valid for geometric-nonlinear analysis. For each factored load case, a separate geometric-nonlinear analysis was

performed using the Newton-Raphson iteration method in which the load was incremented up to a final value of 1.0 times the total factored load. An example of the HL-93 static live load case for the controlling point from the peer reviewer’s analysis (maximum moment-y at Panel Point 18) is shown in Figure 7 below.

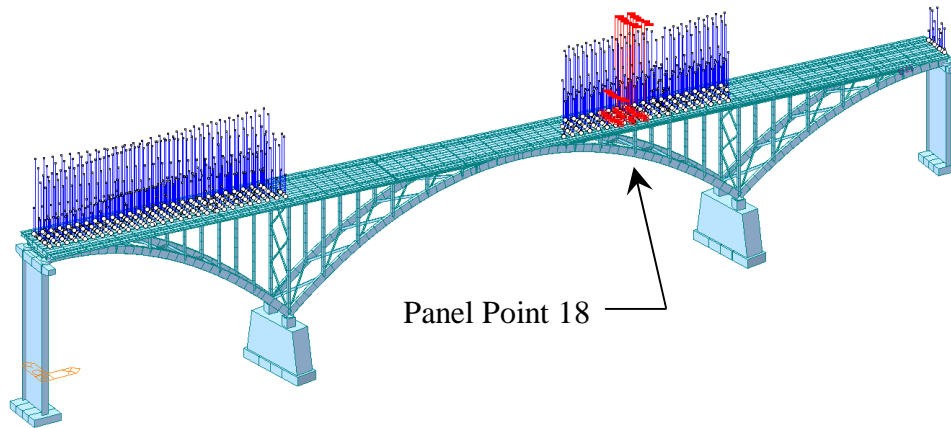


Figure 7: Static Live Load Case for Maximum Moment at PP18

For each panel analyzed using AISC Appendix 1 procedures, the analysis model converged up through a load increment of 1.0 times the factored load, showing that the buckling loads of the arch were greater than factored load demands and that the structure remains stable under factored loads. Following the AISC Appendix 1 provisions for these panels, demands were taken from the final load increment of the geometric nonlinear analysis models, and axial capacity was calculated by taking the nominal compressive strength of members as the cross-section compressive strength $F_y A_g$. Arch rib bending capacities were determined using AASHTO LRFD code equations. The resulting demand-capacity ratios for Strength I loads are shown in Table 3 below. The demand-capacity ratios found using a conventional linear elastic analysis with AASHTO LRFD capacity equations are shown in Table 3 as well, illustrating the significant conservatism of these conventional analysis methods.

Table 3: Controlling Strength I demand-capacity ratios for the arch rib obtained by the peer reviewer

Panel	Concurrent Load Case	Linear Elastic Analysis		Direct Analysis Method	
		Controlling D/C	Rating Factor	Controlling D/C	Rating Factor
PP1-PP2	Max My	0.91	1.24	NOT RUN	
PP2-PP3	Max My	1.02	0.96	0.49	> 1.0
PP3-PP4	Max My	1.11	0.80	0.52	> 1.0
PP4-PP5	Max My	1.12	0.78	0.56	> 1.0
PP5-PP6	Max My	1.15	0.72	0.62	> 1.0
PP6-PP7	Max My	1.23	0.61	0.59	> 1.0
PP7-PP8	Min My w/ Dbl Trk	1.74	0.13	0.61	> 1.0
PP8-PP9	Min My w/ Dbl Trk	1.35	0.43	0.57	> 1.0
PP9-PP10	Max My	1.29	0.55	0.59	> 1.0
PP10-PP11	Max My	1.27	0.62	0.64	> 1.0
PP11-PP12	Max My	1.22	0.65	0.60	> 1.0
PP12-PP13	Max My	1.12	0.79	0.56	> 1.0
PP13-PP14	Max My	1.10	0.83	0.56	> 1.0
PP14-PP15	Max My	0.78	1.58	NOT RUN	
PP15-PP16	Max My	0.85	1.36	NOT RUN	
PP16-PP17	Max My	1.06	0.88	0.65	> 1.0
PP17-PP18	Max My	1.17	0.72	0.65	> 1.0
PP18-PP19	Max My	1.20	0.67	0.68	> 1.0
PP19-PP20	Max My	1.20	0.69	0.65	> 1.0
PP20-PP21	Min My w/ Dbl Trk	1.17	0.68	0.55	> 1.0
PP21-PP22	Min My w/ Dbl Trk	0.87	1.31	NOT RUN	
PP22-PP23	Max My	0.86	1.32	NOT RUN	
PP23-PP24	Max My	0.80	1.46	NOT RUN	
PP24-PP25	Max My	0.75	1.63	NOT RUN	
PP25-PP26	Max My	0.74	1.66	0.49	> 1.0
PP26-PP27	Max My	0.65	2.09	NOT RUN	

Because superposition of forces is not valid for geometric-nonlinear analysis, it is not possible to separate dead and live load force results for the arch rib to calculate exact rating factors for panels analyzed using the AISC Appendix 1 Method. However, it can be shown that if a demand-capacity ratio calculated using demands due to the total factored load is less than 1.0, the rating factor for the same load combination would be above 1.0. This allowed the peer reviewer to demonstrate that the arch would achieve a passing load rating at all panels where the demand-capacity ratios determined using the AISC Appendix 1 Method were below 1.0.

For the permit vehicles evaluated using the Strength II load combination, the minimum required rating factor was 1.1. When the total factored load combination was generated for direct analysis of panels not passing the initial screening for permit loads, an additional factor of 1.1 was applied to the live load. The analysis was therefore run for a load combination of $YDL+TL+1.1*YLL$ for both routine and annual permits. If the force results from this load combination gave demand-capacity ratios less than 1.0, the corresponding rating factor would be greater than 1.1. Using these methods, the peer reviewer concluded that the arch rib achieves passing ratings for the HL-93 loading and all special and routine owner-specified permit trucks for the Strength I and II load combinations, respectively.

4.3 Determining Critical Buckling Loads using Geometric-Nonlinear Analysis

Although the arch was shown to be stable under factored loads, the peer reviewer also sought to determine the margin between factored loads and the buckling loads of the arch. This was accomplished by loading the 3D geometric-nonlinear analysis model of the High Bridge until a loss of stability occurred. Several different live load placements were utilized, including the live load position that maximized moment at the panel point found to be controlling from the AISC

Advanced Analysis Method (Panel Point 18). The loading at each increment of the geometric-nonlinear analysis can be expressed as

$$\text{Applied Load} = [\text{Load Increment Factor}] [1.25DC + 1.0TL + 1.75(LL+IM)] \quad (2)$$

where the post-tensioned tie tendon load (TL) was calibrated such that the ($\text{Load Increment Factor}$)*($1.0TL$) at the last stable step before buckling is equal to 1.0. This was undertaken so that the beneficial stabilizing effects of the tendon loads are not magnified as the dead and live loads are increased beyond 1.0 times the total factored load. For the loading considered, the peer reviewer found that the model lost stability above a load increment factor of 1.5 (or alternatively 1.5 times the factored load, or a loading 50% greater than the factored load). The deflected shape of the model, magnified 10 times, at a load increment factor of 1.5 for the controlling live load placement for Panel 18 is shown below in Figure 8.

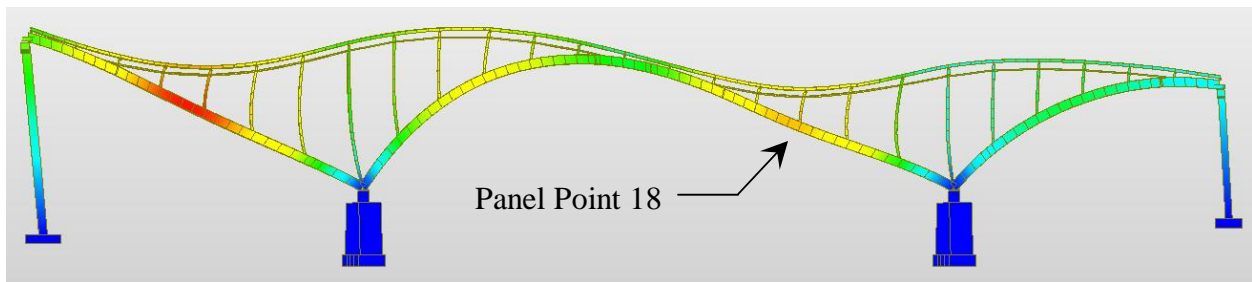


Figure 8: MIDAS/Civil model deformations at (1.5)(Factored Strength I Load at maximizes bending at PP 18)

Figure 9 shows vertical deformations at Panel Point 18 as the load increment factor is increased over the course of the geometric-nonlinear analysis. The plot shows a linear trend line from an equivalent model run with a linear-elastic analysis, where the difference between the two lines represents the second-order effects obtained from the geometric nonlinear analysis.

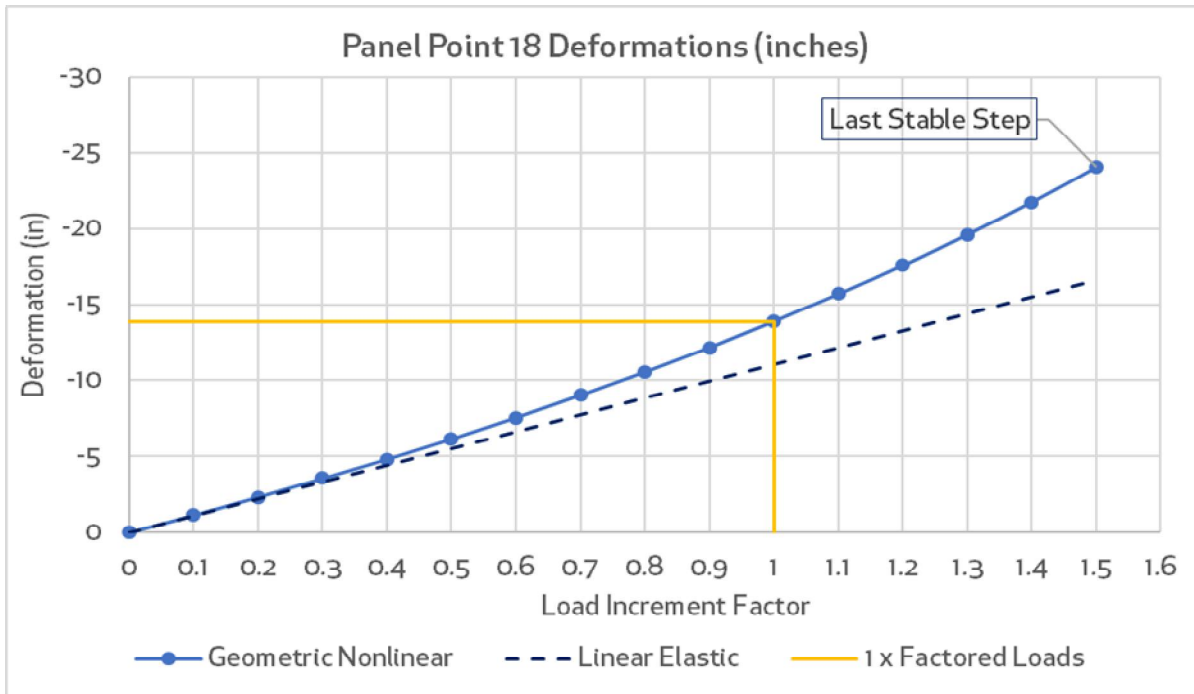


Figure 9: MIDAS/Civil model deformations at Panel Point 18 over the course of geometric-nonlinear analysis

From inspection of Figure 9, second-order effects become significant for deformations as the load approaches the critical buckling load, but are less significant at actual factored and service load levels. In-plane moments follow a similar trend, while the increase in second-order effects for axial forces is less significant as the critical buckling load is approached.

The axial force at Panel Point 18 at buckling for the live load placement that maximizes moment in this panel is approximately 4,500 kips, which is significantly less than the critical buckling load P_e values found by the EOR using eigenvalue analysis and listed in Table 2. A direct comparison, however, between the eigenvalue P_e values and the axial force at buckling obtained from geometric nonlinear analysis is not advisable, since the loading used in the geometric nonlinear analysis was chosen to find the minimum load increment factor at which buckling occurs, (which includes significant bending), while the P_e values are found from an eigenvalue analysis that seeks to obtain buckling loads under a uniform axial loading that minimizes bending. In other words, the critical load increment factor for buckling from geometric-nonlinear analysis occurs under a loading of combined axial force and flexure, while the P_e values found from eigenvalue analysis are for a loading of predominately axial force only.

5. Evaluation of Analyses Results and Conclusions

The controlling panel points and associated maximum demand to capacity (D/C) ratios from each analysis are shown in Table 4. The controlling location for the AASHTO Effective Length Method is located on the Span 3 side of Pier 3 and is controlled by the maximum negative moment at this location. The arch rib transitions from the large arch section to the smaller arch section between Panel Points 7 and 8, with the smaller arch section located on the pier. This fact coupled with the maximum negative moment within the arch rib due to the dual truck case being located over the interior pier results in the controlling location being at this point. Further, the

axial capacity of the smaller arch rib section within Span 3 at 4659 kips is significantly lower than all other axial capacities calculated using the Effective Length Method.

Table 4: Comparison of Controlling Demand/Capacity ratios for the Three Methods

Method	Controlling Panel Point	D/C Ratio
AASHTO Effective Length Method	8	1.26
Eigenvalue Analysis	3	0.94
AISC Direct Analysis	18	0.68

For the eigenvalue analysis method used by the EOR, the controlling D/C ratio of 0.94 is located on the Bay 2-3 side of Panel Point 3. This location is where the arch rib transitions from the smaller arch rib section to the larger arch rib section on the Pier 2 side of Span 3. This, coupled with the large positive moments found within the side spans and the lower axial capacity of Span 3 compared to Span 5, causes the controlling location for the eigenvalue analysis method to be found here.

The D/C ratios calculated using the Effective Length Method were all found to be conservative by a significant margin as compared to the eigenvalue analysis method used by the EOR. The conservatism was expected due to the previously discussed inability of the Effective Length Method to accurately represent the capacity of a continuous arch rib. The eigenvalue analysis method was further found to be conservative when compared to the AISC Direct Analysis Method. The controlling D/C ratio of 0.68 found using the Direct Analysis Method is located at Panel Point 18 within the main span.

The significant fundamental differences between the methods used by the EOR and peer reviewer make it challenging to directly identify the reason for variation in controlling location. However, one potential source of this variation in location is believed to be the conservative load application method used for the eigenvalue analyses. As discussed, the lack of available direction for loading of continuous arches when determining the critical load led to the EOR applying and incrementing a uniform load only to the span of interest for each span in addition to the self-weight of the structure. When compared to the critical loads found when a uniform load is applied to all spans, the side span critical loads are significantly reduced when the stabilizing effect of load applied to the main span is removed. Conversely, when evaluating the critical load of the main span, removing the stabilizing effect of the load on the side spans does not have as significant of an effect. It was expected that the approach used for loading would present a conservative case (primarily for the side spans) and these results provide some confirmation of this assumption. Thus, the apparent conservatism in load application for the side span eigenvalue analyses lead to variation in the controlling location when compared to the Direct Analysis Method.

Use of the eigenvalue analysis method allowed the arch rib to rate for all design and permit live loads. As the eigenvalue method was shown to be conservative as compared to the Direct Analysis Method, eigenvalue analysis was verified as an acceptable means for determining the axial capacity of the arch rib and subsequently deemed acceptable for rating of the arch rib. By

using the eigenvalue analysis method along with the provisions of AASHTO, rating factors were determined for all sections of the arch rib. Further, validation of the eigenvalue method allows for simplified load rating of the structure in the future. Use of the AASHTO provisions allows rating to be conducted for permit vehicles (or any future loads) using linear elastic analyses and further allows for moving load analyses to be used and the results for said analyses enveloped.

For future developments of the AASHTO LRFD and the AISC Direct Analysis codes, the peer reviewer recommends that code writers specify if a minimum margin between the total applied loading that causes loss of global stability and factored demands should be provided when refined analysis techniques such as AISC Direct Analysis are utilized, or if it is only sufficient that the structure remain stable under total factored demands. At present, the ASIC Appendix 1 provisions allow the axial capacity to be taken as $F_y A_g$ as long as the model remains stable under factored demands, and implies that this is acceptable even if global stability is lost at a load increment just above the total factored load. For the rehabilitation of the High Bridge, the EOR, peer reviewer, and owner all concurred that a 1.5 ratio of total applied load at buckling to factored load was acceptable.

Acknowledgments

The analysis results reported here are part of a project funded by the Minnesota Department of Transportation (MnDOT). The authors gratefully acknowledge the funding provided by MnDOT (project sponsor and owner of the bridge).

References

- AASHTO. (2014). "LRFD Bridge Design Specifications, 7th Ed." Washington, D.C.
- AASHTO. (2011). "The Manual for Bridge Evaluation, 2nd Ed." Washington, D.C.
- MnDOT. (2015). "LRFD Bridge Design Manual". Oakdale, MN.
- AISC. (2011). "Steel Construction Manual". Washington, D.C.
- Ziemian, R.D. (2010). "Guide To Stability Design Criteria For Metal Structures". *John Wiley & Sons, Inc., Hoboken, NJ.*